JOURNAL OF THERMOPHYSICS AND HEAT TRANSFER
Vol. 9, No. 4, October–December 1995

Numerical Simulation of Time-Dependent Thermocapillary Convection in Layered Fluid Systems

L. J. Peltier,* S. Biringen,† and M. Farhangnia‡
University of Colorado, Boulder, Colorado 80309

We consider steady and time-dependent thermocapillary convection in encapsulated layers of moderate Prandtl number fluids. Assuming flat free surfaces and fluid/fluid interfaces, the two-dimensional, time-dependent Navier–Stokes equations and the energy equation are integrated by a time-accurate method on a stretched, staggered mesh. Particular attention is focused on the nature of time dependence in water encapsulation of Fluorinert FC-75 and in ethylene glycol encapsulated by FC-75 and hexadecane. We show that similar mechanisms for time-dependent thermocapillary convection exist for single-layer and multiple-layer fluid systems, and that shear effects at a thermocapillary interface can reduce convection in an encapsulated fluid layer. Based on our estimates for the thermal coefficients of interface tension, an apparent benefit of fluid encapsulation is to lessen the tendency toward time dependence.

Nomenclature

AR	=	aspect ratio
C_p	=	specific heat at constant pressure
k	=	thermal conductivity
L_x, L_y	=	x and y dimensions of the cavity
Ma	=	Marangoni number, $\sigma_T \Delta T L_x/\mu\kappa$
$Nu(x)$	=	Nusselt number, Eq. (14)
Pr	=	Prandtl number, ν/κ
p	=	thermodynamic pressure
T	=	temperature
T_{avg}	=	average temperature, $(T_{hot} + T_{cold})/2$
T_{hot}, T_{cold}	=	hot and cold wall temperatures
t	=	time
t_r	=	characteristic time scale
u, v	=	x and y components of the velocity vector
u_i	=	ith component of the dimensionless velocity vector
V_r	=	characteristic velocity scale
x, y	=	coordinate directions
ΔT	=	temperature difference, $T_{hot} - T_{cold}$
$\Delta\psi$	=	fluctuation amplitude, $(\psi_{max} - \psi_{min})$
θ	=	dimensionless temperature, $(T - T_{avg})/\Delta T$
κ	=	thermal diffusivity, $k/\rho C_p$
μ	=	dynamic viscosity
ν	=	kinematic viscosity, μ/ρ
Π	=	period of oscillation
ρ	=	density
σ_T	=	thermal coefficient of surface tension
τ_T	=	thermal coefficient of interface tension
ψ	=	dimensionless stream function
ψ_{avg}	=	average value of ψ, $(\psi_{max} + \psi_{min})/2$
ψ_{max}	=	maximum value of ψ
ψ_{min}	=	minimum value of ψ

Subscripts

I	=	with respect to the fluid below an interface
II	=	with respect to the fluid above an interface

Superscript

n	=	with respect to fluid layer n

Special Symbol

~	=	ratio with respect to the reference property

Received June 6, 1994; revision received March 7, 1995; accepted for publication March 7, 1995.

*Graduate Student, Department of Aerospace Engineering Sciences; currently Research Associate, Department of Meteorology, 503 Walker Building, Pennsylvania State University, University Park, PA 16802. Student Member AIAA.

†Professor, Department of Aerospace Engineering Sciences.

‡Graduate Student, Department of Aerospace Engineering Sciences. Student Member AIAA.

I. Introduction

LIQUID encapsulation is used in crystal growth as a means to eliminate evaporation of volatile components. A consequence of fluid encapsulation is thermocapillary convection in response to interface tension differences caused by thermal gradients along the fluid/fluid interface(s). Although thermocapillary forces are typically small, they can drive large-scale convection when buoyant forces are reduced. Understanding the nature of thermocapillary convection at a fluid/fluid interface is an important step toward the controlled use of the encapsulation technique and toward the design of experiments investigating encapsulation.

To date, few numerical and experimental investigations of thermocapillary convection in multiple-encapsulated fluid layers exist. Notably, Villers and Platten[1,2] reported the decomposition of flow into gravity and thermocapillary-dominated convection cells in water layers encapsulated by heptanol under terrestrial conditions. Furthermore, for generic two-layer systems, the numerical simulations of Crespo del Arco et al.[3,4] and Doi and Koster[5] showed near total suppression of convection in the encapsulated layer through shear interactions between the thermocapillary interface and the return flow in the encapsulant. Peltier and Biringen[6] also demonstrated such thermocapillary communication in their simulation of water encapsulating Fluorinert (FC-75) and showed early results demonstrating time dependence.

The time-dependent response was studied in detail by Peltier and Biringen[7] in their parametric study of thermocapillary convection in single fluid layers of moderate Prandtl number under zero-gravity conditions. They isolated a parameter space eliciting time-dependent responses and described the mechanism sustaining the time dependence. Time dependence in layered fluid systems has not been addressed beyond the early work of Ref. 6.

In this study, we seek to determine if the mechanism leading to time dependence in single fluid layers under zero gravity

is operable in encapsulated fluid systems; we also consider communication across a thermocapillary interface through shear interactions with the flows above and below. Particular attention is given to the suppression of convection in encapsulated fluid layers through these interactions.

We use fully nonlinear, time-dependent, direct numerical simulation to investigate two systems of immiscible fluids that may be used in Earth and space-based experiments: water encapsulation of FC-75 and ethylene glycol encapsulated by FC-75 from below and hexadecane from above. The parameter sets describing these fluid systems are comparable to those used in Ref. 7. Our focus is not a parametric study like that performed in Ref. 7; rather, we present specific cases chosen to demonstrate aspects of time dependence and shear/thermocapillary interactions.

II. Mathematical Model

A. Governing Equations and Boundary/Interface Conditions

We model thermocapillary convection in a rectangular cavity layered with immiscible, incompressible fluids at zero gravity (Fig. 1). Our cross section is far from bounding crossflow walls, and so three dimensionality from viscous interactions is weak. Consequently, our model can capture the lateral thermal-convective instability predicted by Smith and Davis[8] for fluids of moderate to large Prandtl numbers in two dimensions. Following Peltier and Biringen,[7] we assume flat free surfaces and fluid/fluid interfaces; the thermal-convective instability is insensitive to surface deformation. The results of Ref. 7 indicate that the flat surface assumption does not introduce significant errors for a single fluid layer in a tall cavity with fluid properties similar to the ones used here.

We denote each fluid layer using the superscript n. The layer aspect ratio is defined as $\mathrm{AR}^{(n)} = L_x/L_y^{(n)}$, where L_x is the length of the cavity and $L_y^{(n)}$ is the layer depth. The total aspect ratio of the system is $\mathrm{AR} = L_x/L_y$, where

$$L_y = \sum_n L_y^{(n)}$$

In each fluid, we integrate the incompressible Navier–Stokes equations with the thermal energy equation in nondimensional form.

Continuity

$$u_{i,i} = 0 \tag{1}$$

Momentum

$$u_{i,t} + u_j u_{i,j} = -[1/\tilde{\rho}^{(n)}]p_{,i} + \tilde{\nu}^{(n)}(Pr/Ma)u_{i,jj} \tag{2}$$

Energy

$$\theta_{,t} + u_j\theta_{,j} = \tilde{\kappa}^{(n)}(1/Ma)\theta_{,jj} \tag{3}$$

In this index notation, repeated indices are summed and a comma denotes differentiation. The dimensionless velocity, temperature, and pressure are u_i, θ, and p, respectively. In our notation, $(x, y) \equiv (x_1, x_2)$ and $(u, v) \equiv (u_1, u_2)$, where $\boldsymbol{x}_i$ is the coordinate vector. The characteristic scales are $V_r = \sigma_T\Delta T/\mu$ and $t_r = L_x/V_r$ for velocity and time; σ_T is the thermal coefficient of surface tension, μ is the dynamic viscosity, and ΔT is the temperature difference between the "hot" and "cold" walls ($\Delta T \equiv T_{\mathrm{hot}} - T_{\mathrm{cold}}$). The dimensionless temperature is $\theta = (T - T_{\mathrm{avg}})/\Delta T$, where $T_{\mathrm{avg}} \equiv (T_{\mathrm{hot}} + T_{\mathrm{cold}})/2$. For given $\mathrm{AR}^{(n)}$, the Marangoni Ma, and Prandtl Pr, numbers are sufficient to parameterize these flows:

$$Ma = \sigma_T\Delta T L_x/\mu\kappa, \qquad Pr = \nu/\kappa \tag{4}$$

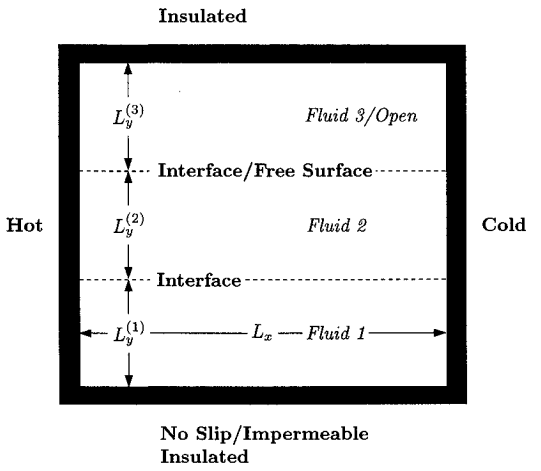

Fig. 1 Schematic of the thermocapillary cavity with aspect ratio AR.

Unless indicated otherwise, we reference all thermophysical properties to the properties of Fluorinert FC-75, denoting their ratios with a tilde. We also use σ_T for FC-75 as the reference property for the thermal coefficients of interface tension τ_T. The remaining thermophysical properties appearing in this problem are the kinematic viscosity ν, the thermal conductivity k, and the thermal diffusivity κ. Estimates of the thermophysical properties for the fluids used in this study are available from the authors upon request.

No-slip and impermeability conditions are imposed at the solid boundaries:

$$u_i = 0 \tag{5}$$

Constant temperature side walls and insulated top and bottom walls are also maintained:

$$\theta = [-1/2,\ 1/2] \text{ at } x = [0,\ 1], \qquad \theta_{,y} = 0 \text{ at } y = [0,\ \mathrm{AR}^{-1}] \tag{6}$$

We enforce impermeability of the upper free surface and the fluid–fluid interface(s) and match the thermocapillary stress to the difference in shear stresses from above (II) and below (I):

$$v = 0, \qquad [\tilde{\mu}u_{,y}]_{II}^{(n)} - [\tilde{\mu}u_{,y}]_{I}^{(n)} = -[\tilde{\tau}_T\theta_{,x}]^{(n)} \tag{7}$$

Shear stresses in the fluid above a free surface are neglected. At the upper free surface and the fluid–fluid interface(s), continuity of temperature and heat flux are ensured:

$$T_{II} = T_I, \qquad [\tilde{\kappa}\theta_{,y}]_{II}^{(n)} - [\tilde{\kappa}\theta_{,y}]_{I}^{(n)} = 0 \tag{8}$$

For a detailed discussion of the interface conditions refer to Peltier.[9]

Values of τ_T are not readily available in the literature, so we estimate them from σ_T data using Antonow's rule.[10] Antonow's rule states that the interface tension τ between a pair of immiscible fluids may be approximated by the difference between the surface tensions σ of each fluid with respect to a passive gas:

$$\tau^{(n)} \approx \sigma_{II}^{(n)} - \sigma_I^{(n)} \tag{9}$$

Assuming a linear temperature dependence for σ, Eq. (9) yields

$$\tau_T^{(n)} \approx [\sigma_T]_{II}^{(n)} - [\sigma_T]_I^{(n)} \tag{10}$$

For the water/FC-75, FC-75/ethylene–glycol, and ethylene–glycol/hexadecane interfaces considered in this study, esti-

mates of τ_T are 4.6×10^{-5}, 6.2×10^{-5}, and 2.4×10^{-5} N/°C^{-1}m^{-1}, respectively.

For data presentation, the stream function ψ and integrated Nusselt number Nu, are extracted from the calculated velocity and temperature fields[7]:

$$\psi_{,x} = -v, \qquad Nu(x) = \int_0^{AR^{-1}} \left(u\theta - \tilde{\kappa}^{(n)} \frac{1}{Ma} \theta_{,x} \right) dy \quad (11)$$

Like Peltier and Biringen,[7] we call a solution converged when the L2-Norm of the horizontal velocity field, the rms value of the difference in u between two consecutive time steps, is less than 10^{-7}. For time-dependent solutions, we check the difference in the maximum absolute value of the stream function between successive periods, which also must be less than 10^{-7}.

B. Solution Procedure and Code Validation

The governing equations are solved on a stretched, staggered mesh using second-order finite differences and time splitting. A third-order Runge–Kutta scheme is used for advancement in time. Chebyshev (cosine) stretching is used in both directions for each layer; thus, for a mesh resolution of 63×63 per layer, a minimum Δx of 6.4×10^{-4} and a minimum Δy of Δx AR^{-1} are formed; single fluid calculations were performed on a 63×63 mesh. Peltier and Biringen[7] present a detailed description of the solution procedure and consider aspects of mesh resolution. From the results of their work, the mesh resolutions in this study were chosen. The present mesh configurations result in continuous and smooth solutions in the vicinity of the bounding solid walls and are sufficient to capture the relevant scales in the problem.

The accuracy of the numerical code was established by comparisons between shear driven, thermally driven, and thermocapillary driven cavity solutions against previously published results. Very good agreement was found in each case.[7]

A set of calculations with varying σ_T/τ_T were conducted to validate the interface conditions. The parameters of the problem were matched to Crespo del Arco et al.[3] For this purpose, an encapsulated fluid layer in an open rectangular cavity was considered. The AR of this system is two, and the layer heights are equal. Both the stream function contours and the maximum horizontal velocities at the free surface and interface were compared with results from Ref. 3. Excellent agreement was found. The maximum and midpoint horizontal velocities at the free surface and at the interface were indistinguishable from those presented in Ref. 3.

III. Results and Discussion

Thermocapillary convection in encapsulated fluid systems under zero-gravity conditions is addressed for open and closed cavities of water encapsulating Fluorinert (FC-75) and for a closed cavity of ethylene glycol encapsulated by FC-75 from below and hexadecane from above (below and above refer to the order of stable stratification under terrestrial conditions). These fluids are chosen since they are immiscible and since their thermophysical data are readily available. Initial conditions for each simulation are obtained from previously converged solutions at lower Ma.

A. Water Encapsulation of Fluorinert FC-75

We compare solutions for water encapsulating FC-75 to single-layer simulations of water and FC-75 under identical geometric and thermal conditions (Ma, Pr, AR) = (1.35×10^5, 6.78, 3.8) for water (based on the properties of water), and (Ma, Pr, AR) = (2.83×10^5, 23.0, 3.8) for FC-75 (based on the properties of FC-75). Referring to the stability diagram of Ref. 7, we find that these parameters for water lie in the unstable regime; thus, we expect (and find) time-dependent flow. In Fig. 2, we present stream function contours and isotherms for this case over one period of oscillation.

The dominant feature of the flow in Fig. 2 is the existence of a strong convection cell throughout the period of oscillation. Following Ref. 7, we use its minimum and maximum strengths during the oscillation, ψ_{min} and ψ_{max}, to define the fluctuation amplitude, $\Delta\psi \equiv (\psi_{max} - \psi_{min})$, and the average strength, $\psi_{avg} \equiv (\psi_{max} + \psi_{min})/2$. Based on successive occurrences of ψ_{max}, we also define a coordinate system ranging from 0 to 2π; π is equally spaced in time between. The period of oscillation Π is the dimensionless time between 0 and 2π. In Fig. 2, instants $\pi/2$, π, $3\pi/2$, and 2π are shown. This oscillation is slow; its period ($\Pi \approx 170$) lasts approximately 25 s, yielding a frequency of oscillation of 0.04 Hz. Values of $\Delta\psi$, ψ_{avg}, and Π for each configuration of water, FC-75, and water encapsulation of FC-75 are summarized in Table 1.

Since the features of the oscillation in Fig. 2 are described in detail by Ref. 7, we only reproduce the highlights. The oscillation is dominated by the formation of a cool finger of fluid drawn from the cold wall and convected beneath the strong convection cell dominant at instants 0 and 2π, Fig. 2(iv); the cool finger deflects upward near the hot wall interacting with temperature-sensitive free surface and instigating the thermal perturbation leading to the oscillatory response; the cell retracts toward the hot wall weakening the siphon, and the monocellular state is re-established.

The layer of FC-75 is also time-periodic, showing similar behavior to the oscillation in water. Since Pr for FC-75 is much larger than Pr for water, the nature of this response may be general. The primary convection cell for the layer of FC-75, however, is confined more closely to the heated wall at corresponding instants in its period and Π is nearly 2.5 times longer than for water; $\Pi \approx 424$, which gives a period of 62 s and a frequency of 0.016 Hz. For the layer of FC-75, ψ_{avg} and in $\Delta\psi$ are only 44 and 29% of the corresponding values for water (see Table 1).

Water encapsulation of FC-75 under these conditions (Figs. 3 and 4) is also time-dependent; $\Pi \approx 190$, which is similar to the 170 found for water and very different from the 424 found for FC-75, suggesting that the time dependence of water is dominant. A comparison of the stream function contours and isotherms for the water layer in Fig. 3, with the contours for the single layer of water (Fig. 2), supports this premise. Each structure from the cool finger and primary convection cell to the secondary and tertiary convection cells is found in the encapsulated simulation. Although it appears that the water layer drives the time-dependent response, ψ_{avg} and $\Delta\psi$ (Table 1), for this layer are only 48 and 38% of their values in the

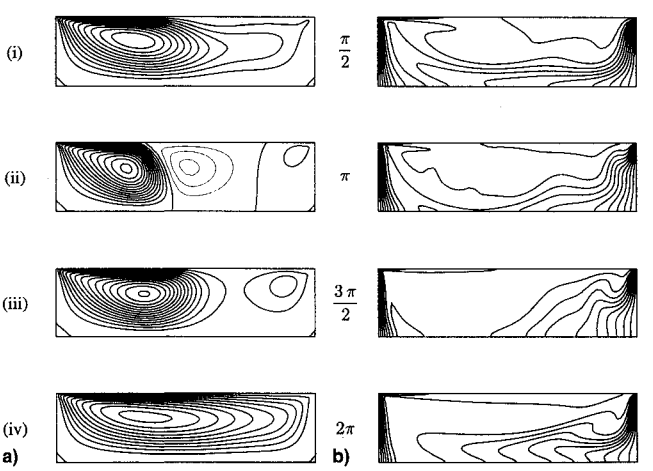

Fig. 2 a) Streamlines [contour interval (CI) 1.0] and b) isotherms (CI = 0.0625) over one period of oscillation in an open cavity of water (Ma, Pr, AR) = (1.35×10^5, 6.78, 3.8). Instants i, $\pi/2$; ii, π; iii, $3\pi/2$; and iv, 2π are presented.

Table 1 Summary data for unsteady simulations of water, FC-75, and water encapsulating FC-75 under zero gravity and identical thermal conditions

	Ma, $\times 10^{-5}$	$\Delta\psi$, $\times 10^{4}$	ψ_{avg}, $\times 10^{4}$	Π	Grid/layer
Open cavity					
Water	1.35	5.057	13.74	170.0	63 × 63
FC-75	2.84	1.478	6.048	423.5	63 × 63
Water/FC-75[b]	2.84	1.924	6.647	189.4	45 × 45
Closed cavity					
Water/FC-75[a]	17.0	6.560	25.18	102.0	45 × 45
[b]		3.195	14.16	——	45 × 45

[a]In the FC-75 layer. [b]In the water layer.
Note: The layer AR is 3.8. Ma for the open cavity is based on σ_T for FC-75, while Ma for the closed cavity is based on τ_T.

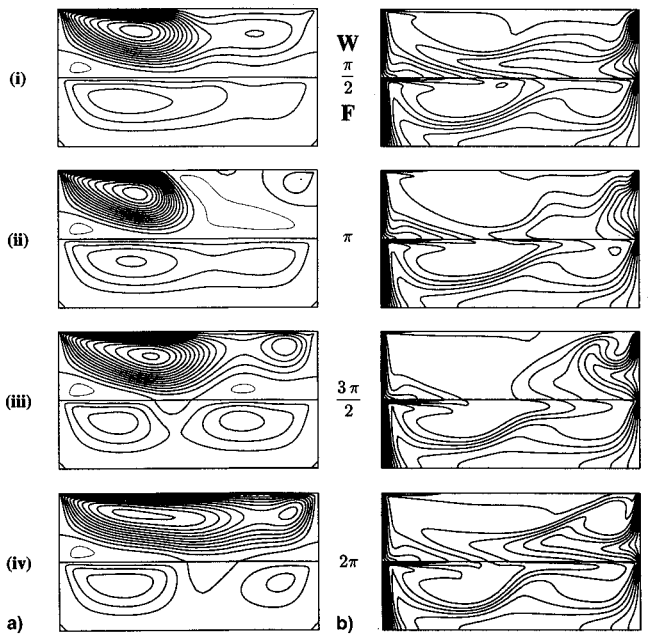

Fig. 3 a) Streamlines (CI = 0.5) and b) isotherms (CI = 0.0625) over an approximate period of oscillation for an open cavity of water *W*, encapsulating FC-75 *F* at instants i, $\pi/2$; ii, π; iii, $3\pi/2$; and iv, 2π. The layer AR and thermal conditions are identical to the single layer simulation (Fig. 2).

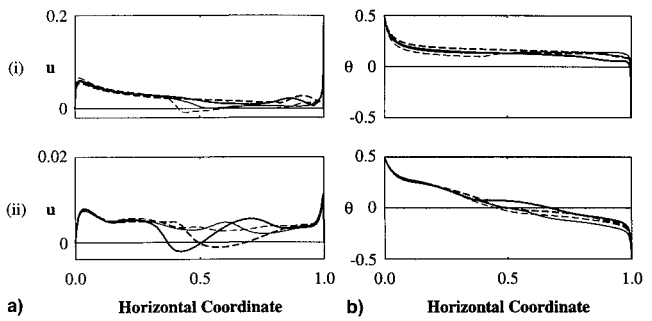

Fig. 4 Free surface/interface profiles of a) u and b) θ at (i) the free surface of the water layer and (ii) the water/FC-75 interface (see Fig. 3). Instants $\pi/2$, π, $3\pi/2$, and 2π are represented by the solid, dashed, bold, and bold-dashed lines, respectively.

single layer. Apparently, the resistance of the opposing stresses from the thermocapillary interface reduces the convection; the increased Π (Table 1) is consistent with the weaker convection.

Thermocapillary convection in the encapsulated layer of FC-75 is weak, [Fig. 4(ii)]. A shear driven cell with opposite sense of rotation develops in the FC-75 layer in response to a communication of shear stresses across the thermocapillary interface. That this cell is not sustained by thermocapillary forces is shown in the temperature profile, Fig. 4b(ii), which decreases monotonically along the interface; thermocapillary responses are toward the cold wall resisting the formation of this cell.

To answer whether an interface alone could instigate an oscillatory thermocapillary response, we closed the water encapsulating FC-75 isolating the thermocapillary interface as the sole source for convection. By increasing τ_T by a factor of 6, we were able to elicit a time-periodic response whose features in each layer followed the familiar response detailed in Fig. 2. Summary data are provided in Table 1.

B. Ethylene Glycol Encapsulated by FC-75 and Hexadecane

We examine responses to two interfaces by considering a closed cavity of ethylene glycol encapsulated by FC-75 from below and hexadecane from above. For these flows, $[Pr, AR^{(n)}] = (23.0, 6.25)$, referenced to the properties of FC-75. Four values of Ma are investigated, each yielding a steady response: 1.24×10^5, 3.75×10^5, 7.46×10^5, and 11.2×10^5. The results are summarized in Table 2. For steady solutions, the Nu across the cavity should be constant. The maximum difference between each Nu distribution presented in Table 2 and its average is 4%, confirming that the solutions are steady and demonstrating that our 45 × 45 and 63 × 63 mesh resolutions are adequate. Poorly resolved simulations show strong variations in Nu across the cavity.

Stream function contours and isotherms for the $Ma = 3.73 \times 10^5$ and 7.46×10^5 simulations are shown in Fig. 5. Thermocapillary responses at the ethylene–glycol/FC-75 interface are dominant (its τ_T is 2.6 times greater than τ_T at the hexadecane/ethylene–glycol interface), driving strong convection in the FC-75 and ethylene–glycol layers. The flow in the ethylene–glycol layer is attenuated due to thermocapillary responses at the hexadecane/ethylene–glycol interface resisting its return flow to the ethylene–glycol/FC-75 interface. Thermocapillary effects on the ethylene–glycol layer from the hexadecane/ethylene–glycol interface are especially pronounced in Fig. 5(ii); the layer has separated into two regions, each influenced most strongly by its neighboring interface.

Near quiescence is observed in the hexadecane layer, ostensibly because the opposing stresses of the return flow in the ethylene–glycol layer and the thermocapillary stresses from the hexadecane/ethylene–glycol interface nearly balance. This conclusion is supported by the data. The isotherms in Fig. 5 and the temperature profile along the interface [Fig. 6b(i)] are almost conductive; therefore, the temperature gradient is constant and a thermocapillary stress exists. Since the velocity field in the hexadecane layer is weak [Figs. 5a(i) and 5a(ii)], the thermocapillary stresses from the interface must be balanced by shear stresses in the ethylene–glycol layer. This balance suggests that the effect of deepening the ethylene–glycol layer would be to increase the convection in the hexadecane layer, since the opposing stresses imparted to the thermocapillary interface by the return flow from the primary

Table 2 Summary data for steady simulations of ethylene glycol encapsulated by FC-75 from below and hexadecane from above

	Ethylene–glycol/FC-75 interface				Hexadecane/ethylene–glycol interface			$Nu(x)$			
Ma, $\times 10^{-5}$	ψ_{min}, $\times 10^4$	u_{max}, $\times 10^4$	x_{max}	u_{mid}, $\times 10^4$	u_{max}, $\times 10^4$	x_{max}	u_{mid}, $\times 10^4$	0.0	0.5	1.0	Grid/layer
1.24	0.276	13.2	0.955	1.11	2.59	0.0612	0.530	2.15	1.98	2.07	45 × 45
3.73	0.210	17.3	0.990	8.31	3.41	0.0734	0.070	3.75	3.93	4.04	63 × 63
7.46	0.163	20.1	0.998	6.37	3.44	0.0734	0.936	5.85	5.74	5.97	63 × 63
11.2	0.140	22.9	0.999	5.48	3.27	0.0612	1.65	7.54	7.60	7.50	45 × 45

Note: Ma is based on σ_T for FC-75. We present the core strength of the primary convection cell ψ_{min}, the maximum interfacial velocity and its position u_{max} and x_{max}, the midpoint interfacial velocity u_{mid}, the integrated Nusselt number at the hot and cold walls and at the midsection of the cavity $Nu(x)$, and the grid resolution.

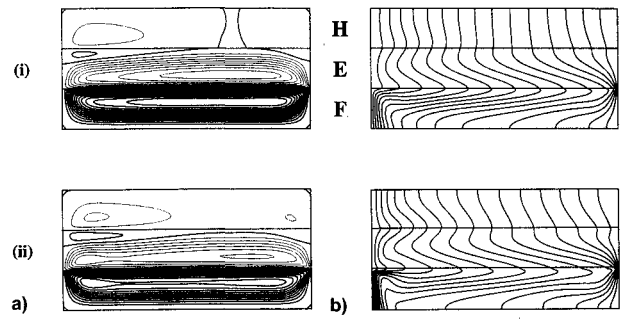

Fig. 5 a) Streamlines (CI = 0.015) and b) isotherms (CI = 0.0625) for ethylene glycol encapsulated by FC-75 from below and hexadecane from above. *F*, *E*, and *H* denote FC-75, ethylene glycol, and hexadecane, respectively: (i) $Ma = 3.73 \times 10^5$ and (ii) $Ma = 7.46 \times 10^5$.

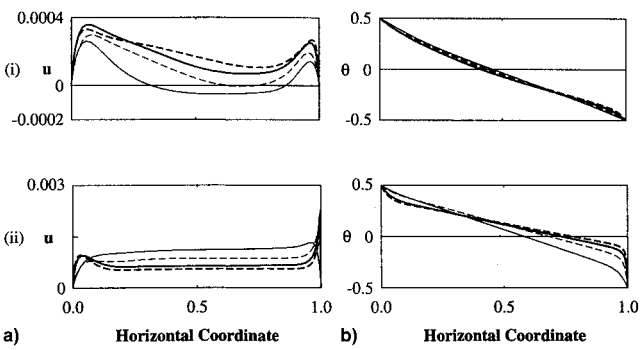

Fig. 6 Interface profiles of a) u and b) θ at (i) the hexadecane/ethylene–glycol interface and (ii) the ethylene–glycol/FC-75 interface. Increasing Ma are identified by solid, dashed, bold, and bold-dashed lines, respectively.

convection cell in the ethylene–glycol would be weakened. The effects of aspect ratio will be considered in a different study.

With increasing Ma, convection in the hexadecane layer increases and the horizontal velocity and temperature profiles shown in Fig. 6 become similar. Since stabilization of the flow in this layer is observed only within a limited parameter range, we find that use of encapsulation to quiet convection is complicated and may not be easily controlled. A different, important application of fluid encapsulation, however, may be to reduce the tendency toward time dependence; estimated values of τ_T are smaller than the values of σ_T from which they are derived.

IV. Conclusions

We have explored details of steady and time-dependent thermocapillary convection in encapsulated and doubly encapsulated fluid systems at zero gravity using τ_T values estimated from σ_T data using Antonow's rule.

Our simulations of water encapsulating FC-75 have demonstrated that the thermal-convective oscillation characterizing time-dependent thermocapillary responses in single fluid layers is also present in the encapsulated systems. We were able to find this response for both free surface and interface driven flows. We also found evidence that convection in the encapsulated layer can be modified by shear forces passed across the fluid–fluid interface; the nature of this effect, however, is complicated and may not be easily controlled.

From simulations of ethylene glycol encapsulated by FC-75 and hexadecane, we showed that fluid quiescence can be achieved by retarding thermocapillary forces through shear interactions. With increases in thermocapillary activity, however, the extent to which convection could be suppressed diminishes.

Each of our findings are subject to the accuracy of our estimates for τ_T. In general, Antonow's rule predicts values of τ_T smaller than the values of σ_T from which they are computed; thus, thermocapillary stresses at a fluid–fluid interface are anticipated to be weaker than the thermocapillary stresses at a free surface. In addition, the effect of the interface on a particular fluid layer is weakened, since the thermocapillary stresses from the interface are shared between both layers. With these effects in mind, a substantial benefit from encapsulation appears to be stabilizations of a fluid layer with respect to time dependence because of the weakened thermocapillary influence.

Acknowledgments

This work was conducted while the first author was supported by the NASA Graduate Researchers Program through NASA Lewis Research Center. Support was also provided by NASA Grant NAG3-1094. The authors would like to thank J. N. Koster for helpful discussions concerning this work.

References

[1]Villers, D., and Platten, J. K., "Coupled Buoyancy and Marangoni Convection in Acetone: Experiments and Comparisons with Numerical Simulations," *Journal of Fluid Mechanics*, Vol. 234, 1992, pp. 487–510.

[2]Villers, D., and Platten, J. K., "Thermal Convection in Superposed Immiscible Liquid Layers," *Applied Scientific Research*, Vol. 45, 1992, pp. 145–152.

[3]Crespo del Arco, E., Extremet, G. P., and Sani, R. L., "Thermocapillary Convection in a Two-Layer Fluid System with Flat Interface," *Advances in Space Research*, Vol. 2, No. 7, 1991, pp. 129–132.

[4]Crespo del Arco, E., Extremet, G. P., and Sani, R. L., "Steady Thermocapillary Flows in a Two-Layer Liquid System with Flat Interfaces," *Journal of Crystal Growth*, Vol. 126, Nos. 2/3, 1993, pp. 335–346.

[5]Doi, T., and Koster, J. N., "Thermocapillary Convection in Two Immiscible Liquid Layers with Free Surface," *Physics of Fluids A*,

Vol. 5, No. 8, 1993, pp. 1914–1927.

[6]Peltier, L. J., and Biringen, S., "Time-Dependent Thermocapillary Convection in Multiply Layered Fluid Systems," *Bulletin of the American Physical Society*, Vol. 36, 1991, p. 2638.

[7]Peltier, L. J., and Biringen, S., "Time-Dependent Thermocapillary Convection in a Cartesian Cavity: Numerical Results for a Moderate Prandtl Number Fluid," *Journal of Fluid Mechanics*, Vol. 257, 1993, pp. 339–357.

[8]Smith, M. K., and Davis, S. H., "Instabilities of Dynamic Thermocapillary Liquid Layers. Part 1. Convective Instabilities," *Journal of Fluid Mechanics*, Vol. 132, 1983, pp. 119–144.

[9]Peltier, L. J., "Numerical Simulation of Time-Dependent Thermocapillary Convention in Layered Fluid Systems," Ph.D. Dissertation, Univ. of Colorado, Boulder, CO, 1992.

[10]Bikerman, J. J., *Physical Surfaces*, Academic, New York, 1970, p. 122.